High-Power math xmlns="http://www.w3.org/1998/Math/MathML" display="inline" overflow="scroll">mi>X/mi>/math>-Band Relativistic Backward-Wave Oscillator with Exceptional Synchronous Regime Operating at an Exceptional Point

Tarek Mealy, Ahmed F. Abdelshafy, and Filippo Capolino

Phys. Rev. Applied **15**, 064021 — Published 8 June 2021

DOI: 10.1103/PhysRevApplied.15.064021

High Power X-band Relativistic Backward-Wave Oscillator with Degenerate Synchronous Regime Operating at an Exceptional Point

Tarek Mealy,* Ahmed F. Abdelshafy,† and Filippo Capolino‡
Department of Electrical Engineering and Computer Science
University of California, Irvine, California 92697, USA

An exceptional point of degeneracy (EPD) is induced in a system made of a linear electron beam interacting with an electromagnetic (EM) guided mode in a vacuum tube made of a corrugated circular metallic waveguide with distributed output ports. This scheme enables a degenerate synchronous regime in backward wave oscillators (BWOs) where the electron beam provides distributed gain to the EM mode with distributed power extraction. Particle-in-cell simulation (PIC) results demonstrate that the proposed EPD-BWO has a starting-oscillation current that scales quadratically with BWO length to a non-vanishing value, which does not occur in standard BWOs and demonstrates the occurrence of the EPD and hence the degenerate synchronism operational regime. The degeneracy of two interactive hybrid modes is also verified by observing the coalescence of their complex-valued wavenumbers at the EPD frequency. Observations on the kinetic energy distribution of the electrons along the BWO demonstrate that the proposed EPD-BWO regime is capable of achieving higher power conversion efficiency at higher levels of power generation due to its ability of maintaining the synchronism for longer BWO lengths compared to the standard BWO regime of operation.

I. INTRODUCTION

An exceptional point of degeneracy (EPD) is here demonstrated in a system made of an electron beam interacting with an electromagnetic (EM) guided mode. The characterizing feature of an exceptional point is the spectral singularity resulting from the degeneracy of at least two eigenstates. We stress the importance to refer to it as "degeneracy" as implied in [1]. Despite most of the published work on EPDs are related to parity time (PT) symmetry [2, 3], the occurrence of EPDs does not necessarily require a system to satisfy the PT symmetry condition, however, in several case it involves a system to simultaneously have gain and loss [4]. The system we consider in this paper involves two complete different media that support waves: an electron beam (e-beam) that supportsspace charge waves and a waveguide that supports EM waves. Exchange of energy occurs when an EM waves in a slow wave structure (SWS) interacts with the e-beam. In this paper the degeneracy condition is enabled by the distributed power extraction (DPE) from the SWS waveguide as shown in Fig. 1. The energy that is extracted from the e-beam and delivered to the guided EM mode is considered as a distributed gain from the SWS perspective, whereas the DPE represents extraction "losses" and not mere dissipation [5, 6].

Backward-wave oscillators (BWOs) are high power sources where the power is transferred from a very energetic e-beam to a synchronized EM mode [7]. The extracted power in a conventional BWO is usually taken at one end of the SWS [8, 9] as shown in Fig. 1(a). One challenging issue in BWOs is the limitation in power generation level. Indeed conventional BWOs exhibit small starting beam current (to induce sustained oscillations) and limited power efficiency without reaching very high output power levels [10]. Several techniques were proposed in literature to enhance the power conversion efficiency of BWOs by optimizing the SWS and its termination. For example, non-uniform SWSs were proposed to enhance efficiency of BWOs in [11], in [12] a resonant reflector was used to enhance efficiency to about 30%, and a two-sectional SWS was also proposed to enhance the power efficiency in [13]. These were optimization techniques. Here, instead, we demonstrate the effectiveness of a regime of operation of a BWO based on a mechanism not utilized yet in contest of BWOs, i.e., exploiting the properties pertaining to the physics of an EPD realized using a DPE scheme as depicted in Fig. 1(b). We refer to a BWO that is operating at an EPD, like the one in Fig. 1(b), as an EPD-BWO. In this paper we show the physical mechanism of an EPD arising from the interaction of an e-beam and and EM wave in a SWS and we show how this finding can be used as a regime of operation in what we call an EPD-BWO to produce very high power with high efficiency.

In our previous work in [5] a theoretical and idealistic analysis of EPD-BWOs based on a generalized Pierce model [14] was presented. Here, the demonstration of the EPD-BWO physical mechanism, is provided in a realistic system as the one in Fig. 1(b) using particle-in-cell (PIC) simulations. PIC simulations provide some of the most accurate results available from the state of the art modeling techniques of realistic vacuum electronics devices and by many are regarded as an essential step toward the experimental demonstration of a prototype. A realistic interaction between an electromagnetic wave and an electron beam is investigated in a cylindrical metallic SWS with various extraction ports as shown in Fig.

* tmealy@uci.edu
† abdelsha@uci.edu
‡ f.capolino@uci.edu

1(b). This paper proves the existence of the EPD in such a system by first demonstrating the asymptotic trend of the *starting* e-beam current that decreases quadratically with SWS length to a non-vanishing value, which was predicted theoretically in [5] and here demonstrated using accurate PIC simulations. In this paper, we also derive an important formula that estimates the value of the e-beam current that generates the EPD (it was not provided in [5]). Besides the observed unconventional trend of the starting current peculiar of the occurrence of an EPD, using PIC simulation, we also show the degeneracy of the complex-valued wavenumbers of two hybrid modes (EM waves interacting with the electron beam) in the realistic waveguide system when the beam dc current is set to specific value at a specific frequency. We provide the performance of the EPD-BWO in terms of output power and power efficiency: they greatly exceed those provided by a comparable conventional design of a BWO Fig. 1(a). We show the main physical reason behind the high power conversion efficiency associated with the proposed EPD-BWO regime by observing the electrons kinetic energy distribution along the SWS using PIC simulations. We observe that the EPD-BWO better maintains the synchronism and electron coherence over the SWS length as compared to standard BWOs and therefore allows higher level of power conversion. Therefore this paper not only demonstrates the physical existence of an EPD in a vacuum tube with distributed power extraction, by means of accurate PIC simulations, it also shows a design of an EPD-BWO and its great potentials in terms of very high power generation and efficiency.

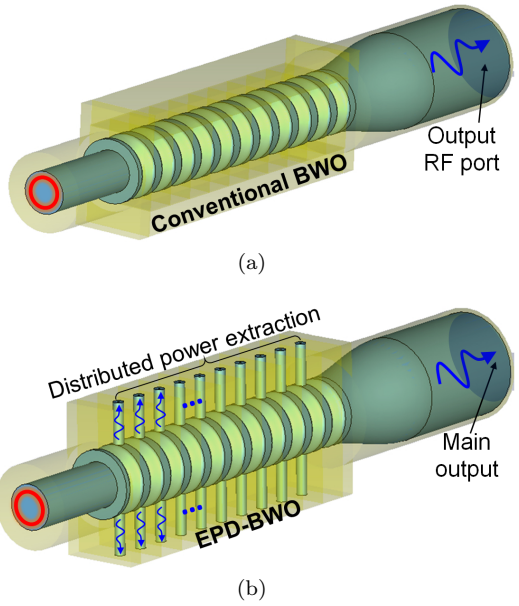

FIG. 1. (a) Conventional BWO where the power is extracted from the waveguide end; (b) EPD-BWO where the power is extracted in a distributed fashion to satisfy the EPD condition. The power is extracted using distributed wire loops (as an example) that are connected to coaxial waveguides.

II. FUNDAMENTAL CONCEPTS: EPD IN THEORETICAL PIERCE-BASED MODEL

The interaction between the e-beam charge wave and the EM wave in the SWS occurs when they are synchronized, i.e., when the EM wave phase velocity $v_{ph} = \omega/\beta_p$ is matched to the average velocity of the electrons u_0, where β_p is the phase propagation constants of the "cold" EM wave, i.e., when it is not interacting with the e-beam. The synchronization condition provides an estimate of the oscillation frequency of BWO ($\omega \approx u_0\beta_p$) and is considered as an initial criterion, because the phase velocity of the "hot" modes, i.e., in the *interactive* system, are different from v_{ph} and u_0 due to the interaction [14, 15].

The interaction between the e-beam and the EM wave in vacuum tube devices was theoretically studied by Pierce in [14]. Assuming a wave eigenfunctions of the interactive system of infinite length in the form of $\phi(z,t) \propto e^{i\omega t - ikz}$, Pierce showed that the solutions of the linearized differential equations that govern the electron beam charges' motion and continuity in presence of the SWS EM field yield four eigenmodes whose dispersion relation is given by the following characteristic equation [14, 15]

$$D(\omega,k) = k^4 - 2\beta_0 k^3 + \left(\beta_0^2 - \beta_p^2 + \frac{I_0 Z_c \beta_p \beta_0}{2V_0}\right) k^2 + 2\beta_0\beta_p^2 k - \beta_0^2\beta_p^2 = 0, \tag{1}$$

where $\beta_0 = \omega/u_0$ is the unmodulated beam wavenumber, V_0 and I_0 are the e-beam equivalent dc voltage and dc current, respectively, and Z_c is characteristic impedance of the cold EM mode. The Pierce model has been extended in Ref.[5, 6] to the case of a SWS with DPE, where the propagation constant and characteristic impedance of the cold EM mode are complex: $\beta_p = \beta_{pr} + i\beta_{pi}$ and $Z_c = Z_{cr} + iZ_{ci}$.

A second order EPD occurs in the interactive system when two solutions of (1) are identical, $k_1 = k_2 = k_e$, where k_e is the degenerate wavenumber, at a given angular frequency ω_e. This yields that *two* hot modes have exactly the same phase velocity $\omega/\mathrm{Re}(k_e)$ which means that synchronization is achieved in the interactive system and not in the cold system. The conditions that lead to having two degenerate wavenumbers of hot modes are $D(\omega_e, k_e) = 0$ and $\partial_k D(\omega_e, k)\big|_{k_e} = 0$ [16], which yet is simplified by getting rid of k_e to [5]

$$\left(\frac{\beta_p}{\beta_0}\right)^2 = \left(\sqrt[3]{\frac{I_0 Z_c \beta_p}{2V_0\beta_0}} + 1\right)^3. \tag{2}$$

The above condition represents a constraint involving the operational frequency ω, e-beam dc voltage V_0 and

current I_0, and cold SWS circuit wavenumber β_p and characteristic impedance Z_c to have an EPD.

When DPE occurs in the SWS, the propagation constant and characteristic impedance of the "cold" EM mode (i.e., without coupling to the electron beam) are complex: $\beta_p = \beta_{pr} + i\beta_{pi}$ and $Z_c = Z_{cr} + iZ_{ci}$. The cold propagation constant imaginary part β_{pi} accounts for power attenuation along the SWS due to the leakage of power out of the SWS. Note that $\beta_{pr}\beta_{pi} > 0$ for a "backward" EM wave that is traveling in the cold SWS (we are using the $\exp(i\omega t)$ time dependency which implies that the EM modes propagates as $\exp(-i\beta_p z)$). Since the phase propagation constant β_{pr} is positive, because it has to match the electron beam effective wavenumber $\beta_0 = \omega/u_0$, one has $\beta_{pi} > 0$. Furthermore, for a backward wave with $\beta_{pr} > 0$, one has $Z_{cr} < 0$ since power travels along the $-z$ direction in the cold SWS. Therefore in the above formulas we have that $Z_c\beta_p = (Z_{cr}\beta_{pr} - Z_{ci}\beta_{pi}) + i\,(Z_{ci}\beta_{pr} + Z_{cr}\beta_{pi})$ is complex.

Note that an EPD requires the coalescence of the two eigenvectors associated to the two degenerate eigenvalues as well. This has been proven in Ref. [5] by analytically determining the two eigenvectors and by showing their analytical convergence. Here we want to add another perspective to ensure the system has an EPD, by showing that this strong degenerate condition is related to the description of the two degenerate eigenvelues' perturbation in terms of the Puiseux fractional power expansion [17] that, truncated to its first term, implies $(k_n - k_e) \approx (-1)^n \alpha_1\sqrt{\omega - \omega_e}$ where k_n, with $n = 1, 2$, are the two perturbed wavenumbers in the neighborhood of (ω_e, k_e). The enabling factor for this characterizing fractional power expansion is the fact that at the point (ω_e, k_e) we have $\partial_\omega D(\omega, k_e)\big|_{\omega_e} \neq 0$ and therefore (2) will yield a branch point $(k - k_e) \approx \alpha_1\sqrt{\omega - \omega_e}$ in the dispersion diagram, where $\alpha_1 = \sqrt{-2\partial_\omega D/\partial_k^2 D\big|_{(\omega_e,k_e)}}$ as shown in Ref. [17]. The existence of the Puiseux series results in having a Jordan block in the system matrix which is one of the characterizing features of EPDs, as it was shown in [5] in details, in terms of the two coalescing eigenvectors.

The cold propagation constant imaginary part β_{pi} accounts for power attenuation along the SWS due to the leakage of power out of the SWS as shown in Fig. 1(b). Under the assumption that $|\beta_{pi}| \ll |\beta_{pr}|$ the complex EPD condition in (2) is simplified to

$$I_0 = I_{0e} \approx \frac{128}{81\sqrt{3}} \frac{V_0}{-Z_{cr}} \frac{\beta_{pi}^3}{\beta_0^3}\bigg|_{\beta_{pr}=\beta_0}. \tag{3}$$

A detailed formulation of the derivation and the assumptions used to derive (3) is presented in Appendix A. From a theoretical perspective, the EPD condition is satisfied just by tuning the e-beam dc current I_0 to a specific value which we call EPD current I_{0e} [18]. The EPD condition in (3) shows that the required e-beam dc current I_{0e} increases cubically when increasing the amount of distributed extracted power, which is represented in terms of the imaginary part β_{pi} of the cold SWS's EM mode. The fact that an EPD e-beam current I_{0e} is found for any amount of distributed power extraction, implies a tight (degenerate) synchronization regime is guaranteed for any high power generation. Therefore, in principle the synchronism is maintained for any desired distributed power output, according to the Pierce-based model. Note that this trend is definitely not observed in standard BWOs where interactive modes are non-degenerate and the load is at one end of the SWS (i.e., $\beta_{pi} \approx 0$ in SWSs made of copper without DPE).

The starting current for oscillation in a conventional BWO, where the supported modes are non-degenerate, was theoretically studied in [9]. The *starting oscillation condition* is determined by imposing infinite gain $A_v \to \infty$, where the gain A_v is defined as the field amplitude ratio at the begin and end of the SWS [9]. Accordingly , the starting current of oscillation in a conventional BWO scales with the SWS length ℓ as $I_{st} = \zeta/\ell^3$ [9, 19] , where ζ is a constant. When a BWO with DPE operates in close proximity of the EPD, i.e., when the beam dc current I_0 is close to the EPD current I_{0e}, there are two coalescing modes out of the three interacting modes with positive $\mathrm{Re}(k)$ and they are denoted by $k_1 = k_e + \alpha\sqrt{I_0 - I_{0e}}$ and $k_2 = k_e - \alpha\sqrt{I_0 - I_{0e}}$ [17], where $\alpha = \sqrt{-2\partial_I D/\partial_k^2 D\big|_{(\omega_e,k_e)}}$ is constant. By imposing infinite gain $A_v \to \infty$ for this case, it has been shown in [5] that the starting current of oscillation is determined in term of the EPD current and the SWS length as

$$I_{st}|_{EDP-BWO} = I_{0e} + \left(\frac{\pi}{\alpha\ell}\right)^2. \tag{4}$$

This remarkable result shows that the starting current decreases to the EPD beam current for increasing length of the SWS, in contrast to the starting current in conventional BWOs that vanishes for increasing length of the SWS. The demonstration of these two scaling laws varying the SWS length of a realistic structure as in Fig. 1 is carried out in the next section using PIC simulations.

III. PARTICLE-IN-CELL SIMULATIONS OF DEGENERATE SYNCHRONOUS REGIME IN BWO

We demonstrate the EPD-BWO regime by taking a conventional BWO design operating at X-band shown in Fig. 1(a). The proposed EPD-BWO is shown is Fig. 1(b) where DPE is introduced using distributed wire loops that are connected to coaxial waveguides. The original SWS geometry shown in Fig. 2(a), is a circular copper waveguide with azimuthal symmetry and with inner and outer radii of $R_i = 11.5$ mm and $R_o = 16.5$ mm, respectively, and period $d = 15$ mm. The surface corrugation of SWS in one period is described by a flat surface $R(z) = R_o$ for $0 \le z < w$, where $w = 5$ mm, and a sinusoidal

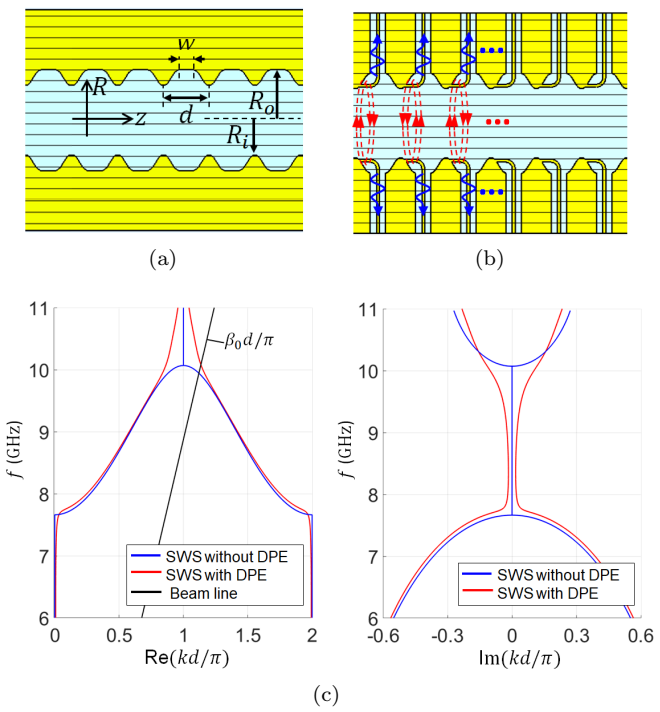

FIG. 2. Details of the longitudinal cross-sections of a SWS without (a) and with DPE (b). (c) Dispersion of EM guided modes in the "cold" SWSs in (a) and (b), without (blue curve) and with (red curve) distributed power extraction (DPE), respectively. The dispersion shows the real and imaginary parts of the complex wavenumber. The non-zero imaginary part of wavenumber (red line) shows that the SWS in (b) exhibits distributed power extraction. The black line is the "beam line" described by $\beta_0 = \omega/u_0$, and the intersection point with the curve of $\beta_{pr} = \mathrm{Re}(\beta_{pr})$ represents the approximative synchronization point.

corrugated surfaces for the rest of the period described as $R(z) = (R_o+R_i)/2+((R_o-R_i)/2)\cos(2\pi(z-w)/(d-w))$ for $w \le z < d$. The whole body of the BWO is made of copper with vacuum inside. The DPE is introduced by adding two wire loops in each unit cell, above and below as shown in Fig. 2(b), that couple to the azimuthal magnetic field (shown in Fig. 3(b)), and by Farady's Law an electromotive force is generated that excites each coaxial waveguide, similarly to the way power is extracted from magnetrons (Ch. 10 in Ref. [7]). The coaxial cables have outer and inner radii equal to 2.57 mm and 0.5 mm, respectively, leading to a 98 ohm characteristic impedance.

A. EM modes in cold SWS

We first analyze the EM modes supported by the two cold SWSs in Fig.2(a) and in Fig. 2(b) (we refer to a "cold" SWS when we do not consider the interaction with the e-beam). Therefore, Fig. 2(c) shows a comparison between the dispersion relation of the EM modes in the two "cold" SWSs: one used in the conventional BWO

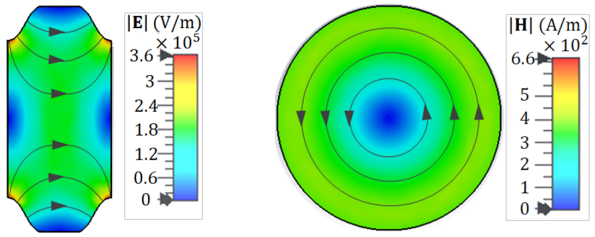

FIG. 3. Field distribution for the TM-like mode supported by the SWS in Fig. 2(a): (a) electric field in a unit cell of the longitudinal cross-section of 2(a), and (b) magnetic field on the transverse cross-section at the largest radius of the corrugated circular waveguide. Fields are found with the mode solver of CST Studio Suite.

in Fig. 2(a), and the other one used in the BWO with DPE in Fig. 2(b). The dispersion diagram shows only the EM mode that is TM-like, i.e., the one with an axial (longitudinal) electric field component, with electric and magnetic field distributions shown in Fig. 3. The dispersion curves in Fig 2(c) show that the EM mode in the cold SWS with DPE is a backward wave that has a propagation constant with non-zero imaginary part β_{pi} at the frequency where the interaction with the e-beam would occur, i.e., at the point where the EM wave phase velocity ω/β_{pr} is synchronized to the relativistic velocity of electrons $u_0 = 0.88c$, where c is the speed of light in vacuum. This means that the cold SWS in Fig. 2(b) is suitable for our design of a BWO with an EPD [5, 6]. The complex wavenumber dispersion relation in presence of DPE, shown in Fig 2(c), is obtained by using two multi-mode ports at the begin and end of a SWS unit-cell where each port has 30 circular-waveguide modes (almost all evanescent) that sufficiently represent the first TM-like Floquet mode in the periodic SWS, while all the coaxial waveguides are matched to their characteristic impedance to absorb all the outgoing power. This is done using the Finite Element Frequency Domain solver implemented in CST Studio Suite by DS SIMULIA that calculates the scattering parameters of the unit cell, that have then been converted to a transfer matrix to get the SWS complex Floquet-Bloch modes following the same method in [20].

B. Existence of EPD-BWO regime

We demonstrate the EPD-BWO regime by considering a conventional BWO operating at X-band whose SWS is shown in Fig. 2(a), with added DPE ports as in Fig. 2(b). An example of the dispersion of the complex-wavenumber modes in the interactive ("hot") EM e-beam system with DPE has been shown in [5, 6] using the Pierce-based model revealing the occurrence of an EPD in an idealize system made of transmission lines. Here in-

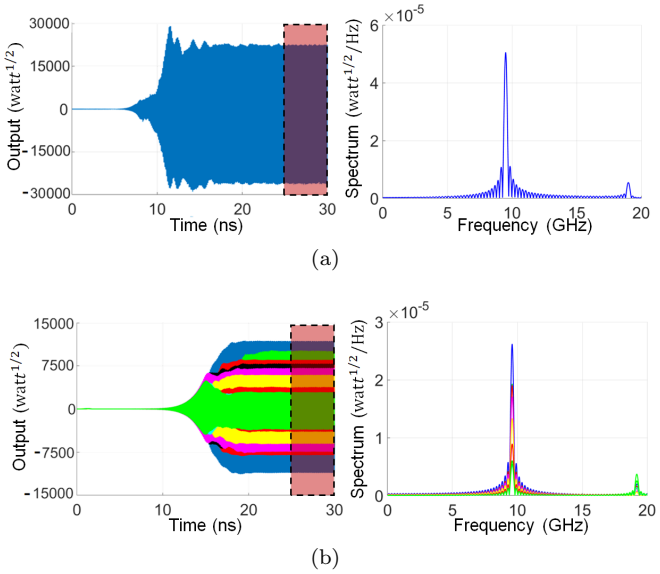

FIG. 4. Output signals and their corresponding spectra for: (a) Conventional BWO where the output power is only extracted from one port as shown in Fig. 1(a). (b) EPD-BWO where power is extracted from multiple ports as shown in Fig. 1(b), they all have the same frequency of oscillations. In both cases, the time-window used for the Fourier transforms is depicted by a rectangle.

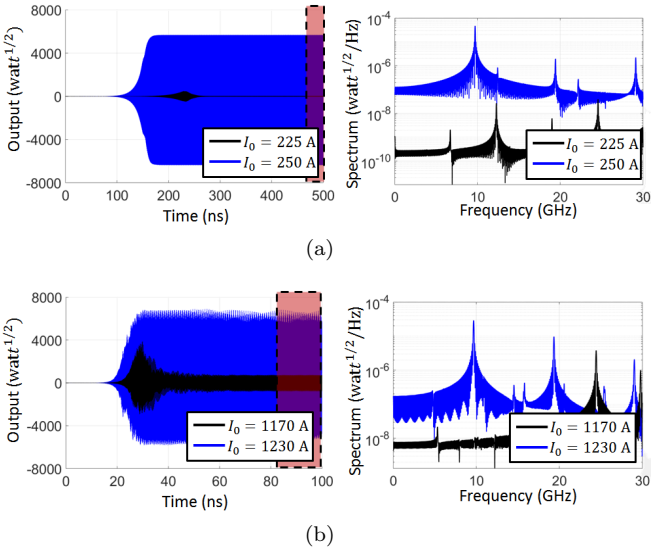

FIG. 5. Output signal at the right-end waveguide port and its corresponding spectrum when the SWS has 11 unit-cells, at (blue) and below (black) the e-beam starting current for: (a) Conventional BWO, and (b) EPD-BWO. The frequency spectrum shows that there is not self-standing oscillation at 9.7 GHz when the e-beam dc current is below the oscillation threshold, i.e., when the current is below 250A for the conventional BWO, and below 1230A for the EPD-BWO, but self-standing oscillation occurs at these two e-beam current values, hence they represent the starting currents for the two types of BWOs. It is important to stress that the figure shows only the output power at the right-end port of the EPD-BWO, and that the output value of the EPD-BWO from only the right-end waveguide port is comparable to the one coming out of the conventional BWO.

stead we provide a concrete demonstration of the EPD-BWO regime in the SWS in Fig. 1(b) using PIC simulations, and resorting to some unique features of the EPD in the e-beam - EM wave interactive system, that supports two degenerate modes in the hot SWS. Simulations based on the PIC solver, implemented in CST Studio Suite, use a relativistic annular e-beam with dc voltage of $V_0 = 600$ kV, inner and outer radii of $R_{ib} = 9$ mm and $R_{ob} = 10.3$ mm, respectively, and with dc axial magnetic field of 2.6 T to confine the electron beam. The cathode is modeled using the dc emission model with 528 uniform emission points. The full-wave simulation uses around 1.3M Hexahedral mesh cells to model the SWS.

The output signals and their corresponding spectra for both BWOs, with and without DPE, are shown in Fig. 4 where a self-standing oscillation frequency of 9.7 GHz is observed when the used beam dc current is $I_0 = 1740$ A for both cases.

We study the starting e-beam current for oscillation in both types of BWO (the conventional one, and the EPD-BWO in Fig. 1) by sweeping the e-beam current I_0 and monitoring the RF power and its spectrum of the waveguide output signal at the right end of the cylindrical waveguide. Using a SWS with 11 unit-cells we show in Fig. 5 the output power at the main port at the right end of the SWS when the e-beam current is just below and just above the threshold current. A self-standing oscillation frequency of 9.7 GHz is observed when the e-beam dc current I_0 for the conventional BWO is at or larger than than 250A, while for the EPD-BWO, self-standing oscillations is observed for an e-beam current I_0 equal or greater than 1230A. Such oscillations are not observed for smaller e-beam current, as for example 225A for the conventional BWO and 1170A for the EPD-BWO. Therefore we conclude that the the starting current of oscillation is approximately 250A for the conventional BWO, and 1230A for the EPD-BWO, when the SWS length is 11 periods.

To assess the occurrence of an EPD we verify the unique scaling trend of the starting current in (4) by repeating the previous study for different SWS lengths. Fig. 6 shows the starting current scaling trends for both conventional BWO and EPD-BWO based on PIC simulation results, varying the number of periods of the SWS. The dashed lines represent fitting curves and the case of EPD-BWO shows very good fitting with 99% R-square. In comparison to a conventional BWO, the EPD-BWO is characterized by a starting current (threshold) that does not tend to zero as the SWS length increases, and a scaling that is a quadratic function of the inverse of the SWS length.

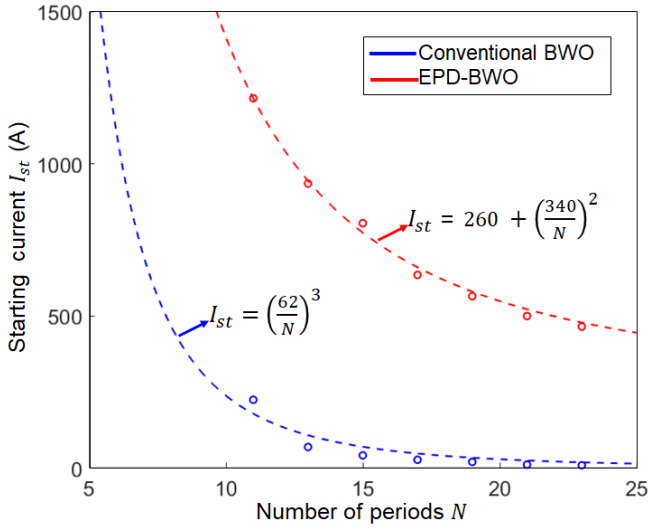

FIG. 6. Scaling of starting e-beam current for oscillation in conventional BWO and EPD-BWO. Dashed lines represent fitting curves. The EPD-BWO shows a starting current trend that does not vanish for long SWS.

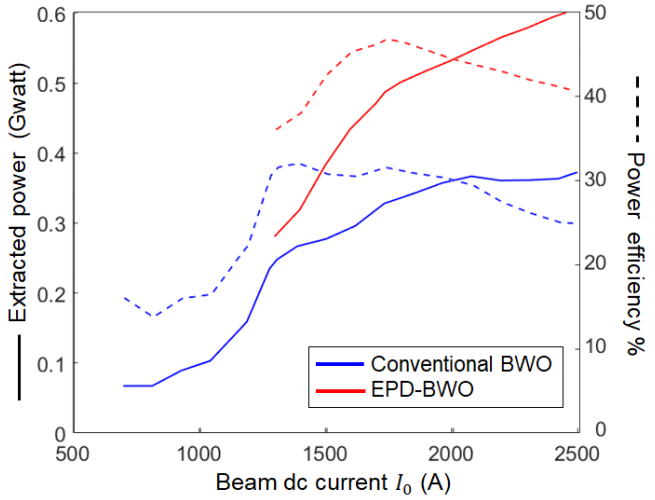

FIG. 7. Comparison between the efficiency of a conventional BWO and an EPD-BWO using $N = 11$. The EPD-BWO shows improved efficiency at higher level of power generation compared to the conventional BWO.

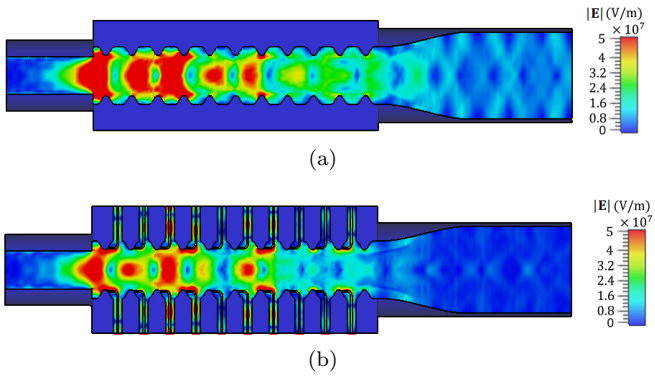

FIG. 8. Electric field distribution in the SWS for: (a) conventional BWO and (b) EPD-BWO. The figure in (b) shows power extraction in distributed fashion from the coaxial waveguides at the top and bottom of the circular waveguide.

C. Power performance: EPD-BWO compared to a conventional BWO

We compare the RF conversion power efficiency (RF output power over dc e-beam power) of the conventional BWO with that of the EPD-BWO in Fig. 7 for e-beam dc currents that exceed the starting current, assuming the SWS has 11 unit-cells. The figure shows that the EPD-BWO has higher efficiency and also higher level of output power compared to a conventional BWO with same dimensions. The results show that the EPD-BWO has a maximum efficiency of about 47% at about 0.5 GW output power (the sum of the power from each output in Fig. 1(b)). Instead, the conventional BWO has a maximum efficiency of about 33% at an output power level of about 0.27 GW. It is important to point out that the EPD-BWO has a higher threshold beam current to start oscillations compared to the conventional one which is in consistent with the theoretical results in [5] and with the requirement of generating higher power levels.

Figure 8 shows the electric field distribution for the conventional BWO and the EPD-BWO when the e-beam dc current I_0 is 1750 A, in both cases, for a SWS of 11 unit cells. The figure shows that for the conventional BWO the power is extracted only from the main port at the right end, whereas for EPD-BWO most of the power is extracted in a distributed fashion from the top and bottom coaxial waveguides, resulting in much high power and high efficiency as demonstrated in Fig. 8.

IV. MAINTAINING SYNCHRONISM AT HIGH POWER LEVELS

The interaction between the electron beam and the guided EM field requires synchronism. Synchronism is achieved when the electrons average velocity and phase velocity of the EM wave supported by the SWS are matched. The power delivered to the EM field in the BWOs is provided by the electrons's kinetic energy. Therefore, extracting more energy from the electron beam would result in further decreasing the average speed of electrons, which in turns leads the system out of synchronism. Consequently, the level of power extraction and the power conversion efficiency would be limited because synchronism is maintained only for finite SWS lengths. The advantage of using the EPD concept in BWOs through introducing DPE is that the synchro-

nism is maintained for higher levels of power extraction as compared to conventional BWOs. To show that, we compare the synchronism in the EPD-BWO regime and in the conventional BWO by performing PIC simulations and monitoring the electrons kinetic energy along the BWO as shown in Fig. IV. PIC simulations are performed for structures with a number of unit-cells $N = 20$ to be able to see the electrons behavior over a large length. The plots in Fig. IV presents the phase plots of electrons

showing the space bunching of electrons . PIC simulator used about 6×10^6 particle charges to model the electron beam, where each particle has a macro-charge of about $q_p = -7 \times 10^6 e$ ($e = 1.602 \times 10^{-19}$ C) that represents a cloud of electrons, where e is the charge of one electron. Each plot in Fig. IV shows the kinetic energy of the electrons along the structure , i.e., each dot in the plot corresponds to the kinetic energy of every electron belonging to a given particle charge at position z. We show first the conventional BWO case when the beam dc current $I_0 = 30$ A is just above the estimated starting current $I_{st} = 29.8$ A. For this case the EM mode-charge wave synchronization is maintained for almost all the SWS length as shown in Fig. 9(a). The electrons energy distribution along the SWS, at a given time instant after reaching the steady state regime, becomes more irregular when we increase the beam dc current as shown in Fig. 9(b) and Fig. 9(c). These figures show that length over which the synchronization and coherence of electron is satisfied, decreases when trying to extract more power by increasing the beam dc current. We now compare the EPD regime with the one of the conventional BWO using the same beam dc current, which is approximately 18 times the starting current of conventional BWO case and approximately equal to the starting current of the EPD-BWO case (I_0 =550 A). The phase space plot of the electrons at a given time instant after reaching the steady state regime in Fig. 9(c) and Fig. 9(d) shows that the EPD-BWO better maintains the synchronism and electron coherence over the whole SWS length as compared to the conventional BWO, at higher power levels. These observations contribute to the explanation of why the EPD-BWO regime leads to higher output power levels and higher power conversion efficiency than those of a conventional BWO. The dashed black line in each figure represents the time-averaged kinetic energy of the electrons at each z-location calculated as $E_{k,avg}(z) = \frac{1}{T}\int_{t=t_{ref}}^{t=t_{ref}+T} E_k(z,t)$, where t_{ref} is any time instant after steady state regime is reached, $T = 1/f$ and f is the oscillation frequency, and $E_k(z,t)$ is equivalent electrons kinetic energy calculated as the mean of electrons energy existing in small proximity of 1 mm window along the coordinate z at time instant t. Comparing Fig. 9(c) and Fig. 9(d), the electrons kinetic energy, and hence the electrons average velocity, is maintained for longer lengths as compared to the BWO with standard regime, and therefore would result in a higher energy transfer and higher power conversion efficiency.

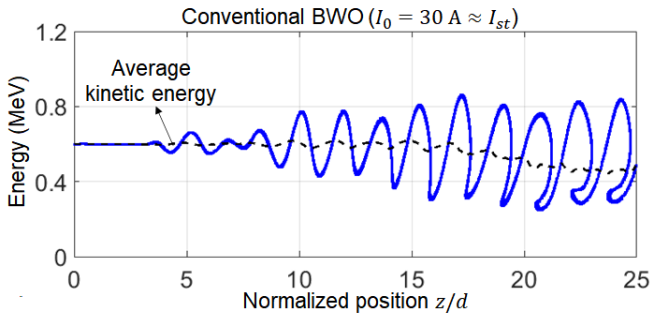

(a)

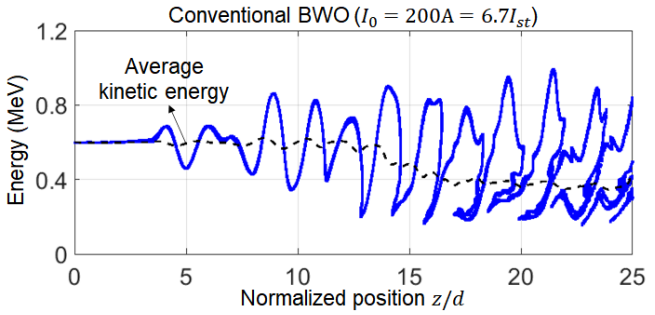

(b)

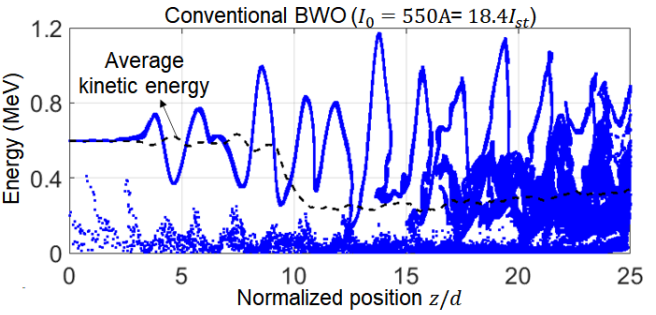

(c)

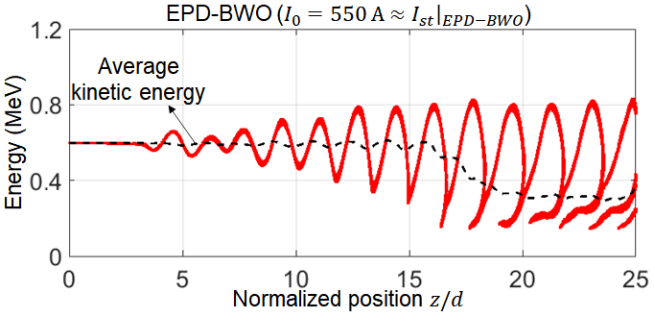

(d)

FIG. 9. Phase space plot of electrons showing the electrons' kinetic energy distribution at a time instant after reaching the steady regime. (a), (b) and (c): conventional BWO when the beam dc current is 30 A, 200 A and 550 A. (d): EPD-BWO when the beam dc current is just above the starting current for oscillation 550 A. (a), (b) and (c) show that synchronism is lost when attempt to increase power extraction level by increasing the beam dc current, whereas for DPE case in (d), synchronism is maintained for a longer SWS length when compared to the conventional BWO in (c), assuming that they use the same beam dc current. The dashed black lines in the figures represent the time-averaged kinetic energy which decreases with growing z-location because of the energy transfer from electron beam to the SWS.

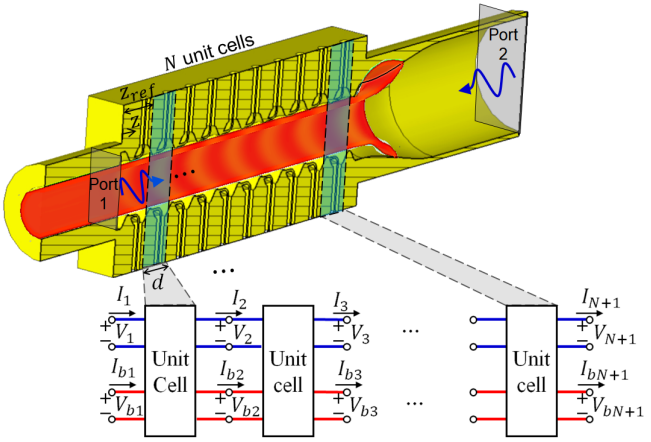

FIG. 10. Setup used to determine the complex wavenumber versus frequency dispersion relation of hybrid modes in hot SWSs based on PIC simulations. Each unit cell in the hot SWS is modeled as a multi-port network circuit with *equivalent* voltages and currents representing EM waves (V_n, I_n) and space-charge waves(V_{bn}, I_{bn}) dynamics.

V. DEMONSTRATION OF DEGENERATE DISPERSION OF HYBRID HOT MODES USING PIC SIMULATIONS

The goal is to verify the degeneracy of the wavenumbers of the modes of the interactive system (i.e, the hybrid modes) in the hot SWS using PIC simulations. Previously, the degenerate dispersion has been shown using the approximate analytical method based on the Pierce model [5]. Here we adopt the general procedure described in [21] to estimate the complex-valued wavenumbers of the interactive (hybrid) modes, and show the hybrid mode degeneracy using data extracted from PIC simulations. The procedure is based on exciting the SWS from both sides by EM waves having monochromatic signal as illustrated in Fig. 10, and then calculating the hybrid-system state vectors that describe the EM field and the electron beam dynamics at discrete periodic locations along the SWS. The time domain data extracted from PIC simulations are transformed into phasors after reaching a steady regime. We then find the transfer matrix of the unit-cell of the "hot" SWS that best relates the calculated state vectors. Once the estimate of the unit-cell transfer matrix is obtained, we find the complex values of the wavenumbers of the hybrid eigenmodes in a hot SWS using Floquet theory. The details ofthe steps used to generate the hybrid-modes dispersion relation in the hot SWS are provided in Appendix B.

The wavenumber-frequency dispersion describing the complex-valued wavenumber of the hybrid eigenmodes in the hot SWS is determined by running multiple PIC simulations of a SWS with 11 unit-cells at different frequencies and then determining the transfer matrix of the unit-cell at each frequency using Eq. (B3). Calculations are based on using a beam dc current of $I_0 = 260$A, which is the value of EPD beam current (pertaining to the infinitely long SWS) according to the fitting shown in Fig. 6; the use of this current value of current should guarantee the coalescence of two interactive modes. It is worth mentioning that the used beam current in this case is below the starting current of oscillation of the hot SWS of 11 uni cells, which is estimated to be 1215 A, therefore, one can model each unit-cell in the structure using a transfer matrix as discussed in Appendix B. The dispersion diagram of the four modes in the hot EM-electron beam system is shown in Fig. 11(a) (solid curves) using 27 frequency points (27 PIC simulations). The dashed red line represents the space-charge wave (i.e., the beam line) of the isolated electron beam. The figure show a degeneracy of both the real and imaginary parts of the wavenumbers of two hybrid modes (the red and blue curves) at a frequency near $f = 9.87$ GHz which is very close to the oscillation frequency. As a further proof, we also verify that the EPD is obtained when the beam dc current is set to a specific value, by observing the wavenumber-beam current dispersion describing the hybrid eigenmodes at $f = 9.87$ GHz, which is the frequency at which we expect to find the EPD. This is shown in Fig. 11(b) where two dispersion curves of the four interactive modes intersect (in their real and imaginary parts) when sweeping the beam current (the red and blue curves). The figure show that the EPD occurs when the beam current is close to 260 A, which is consistent with result in Fig. 6.

VI. CONCLUSION

The physical mechanism of an EPD in a hybrid system where a linear electron beam interacts with an electromagnetic mode has been demonstrated in a BWO made of a circular corrugated waveguide with distributed power extraction. The EPD demonstration is based on using PIC simulations modeling realistic interactions between an electron beam and the EM modes in the waveguide; therefore this paper expands the previous EPD observation in [5] that was made using an approximate analytical method based on the simplistic Pierce model. The manifestation of such EPD is useful to conceive a degenerate synchronous regime for BWOs that have a starting-oscillation current law that decreases quadratically to a given fixed value for long waveguide interaction lengths; as a consequence PIC simulations show higher efficiency and much higher output power than a standard BWO. The unique quadratic threshold scaling law for long waveguide interaction lengths observed in the realistic EPD-BWO setting studied here demonstrates the EPD-based synchronization phenomenon, compared to that in a standard BWO that has a starting-oscillation current law that vanishes cubically. As a further confirmation beyond the observed quadratic scaling law of the threshold current, in this paper we have also shown the complex-valued wavenumber degeneracy in the realistic

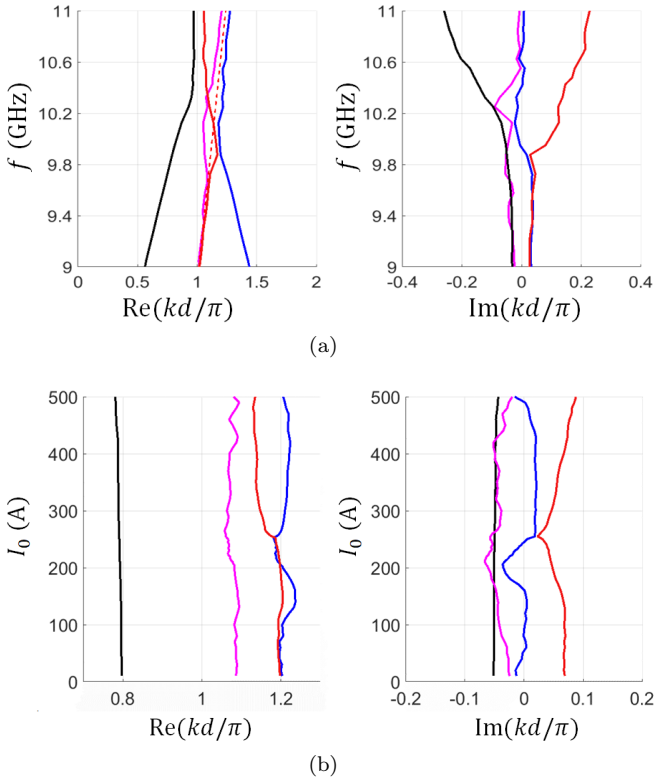

FIG. 11. Dispersion of complex-valued wavenumbers of the four hybrid modes in the hot SWS of 11 unit-cells, estimated from data extracted from PIC simulation : (a) varying frequency when the electron beam dc current is $I_0 = 260$A and (b) varying the beam dc current, at $f = 9.87$ GHz. All the considered beam dc currents used to generate the results in (a) and (b) are lower than the starting current of oscillation, estimated to be 1215 A. The plots show a modal degeneracy (in the real and imaginary parts) when the the beam dc current is $I_0 = 260$A and the operating frequency is $f = 9.87$ GHz

hot SWS with distributed power extraction, elaborating data extracted from PIC simulations. The distributed power extraction concept is useful to generate the EPD and we have shown that the propose degenerate BWO regime leads to higher power extraction and higher power efficiency when compared to a standard BWO. The physical mechanism of why more power can be extracted is also explained in terms of observations made on the distribution of the electrons kinetic energy revealing that the synchronous behavior of the EPD-BWO is mantained for longer SWS lengths and at higher power levels than what observed in a standard BWO

VII. ACKNOWLEDGEMENT

This material is based upon work supported by the Air Force Office of Scientific Research award number FA9550-18-1-0355. The authors are thankful to DS SIMULIA for providing CST Studio Suite that was instrumental in this study.

Appendix A: Electron beam dc current that satisfies the EPD condition

The electron beam current that satisfies the EPD condition is determined by rearranging (2) as

$$I_0 = I_{0e} \equiv \frac{2V_0\beta_0}{Z_c\beta_p}\left(\left(\frac{\beta_p}{\beta_0}\right)^{2/3} - 1\right)^3. \tag{A1}$$

To satisfy the above condition, since the e-beam dc current I_0 is real valued, the imaginary part of the right hand side should vanish, i.e.,

$$\arg\left(\frac{2V_0\beta_0}{Z_c\beta_p}\left(\left(\frac{\beta_p}{\beta_0}\right)^{2/3} - 1\right)^3\right) = 2n\pi,\ n = \{0, \pm 1, ..\}. \tag{A2}$$

The propagation constant and characteristic impedance of the backward EM mode are complex, and the imaginary part $\beta_{pi} > 0$ of the cold propagation constant accounts for distributed power extraction. Under the assumption that $0 < \beta_{pi} \ll \beta_{pr}$ and $|Z_{ci}| \ll |Z_{cr}|$ and considering a backward propagating mode so that $\mathrm{Re}\,(Z_c\beta_p) < 0$, it can be easily shown that $|\mathrm{Re}\,(Z_c\beta_p)| > |\mathrm{Im}\,(Z_c\beta_p)|$.

By assuming that the EPD point at $(\omega, k) = (\omega_e, k_e)$ is close to the synchronization point of the non interactive diagrams (that is $(\omega, \beta_p) \approx (\omega, \beta_0)$) , i.e., we impose that at $\omega = \omega_e$ one has $\beta_p = \beta_0(1 + \delta)$, where $\delta = \delta_r + i\delta_i$, and $\delta_i > 0$ (because of losses and DPE in the cold SWS supporting the backward mode). Because we assume that both $|\delta_r| \ll 1$ and $\delta_i \ll 1$, the argument of the complex value in (A2) is dominated by the latter term, i.e.,

$$\arg\left(\frac{2V_0\beta_0}{Z_c\beta_p}\left(\left(\frac{\beta_p}{\beta_0}\right)^{2/3} - 1\right)^3\right) \approx \pi + 3\arg\left(\left(\frac{\beta_p}{\beta_0}\right)^{2/3} - 1\right). \tag{A3}$$

The cubic root in (A3) has three solutions:

$$\left(\frac{\beta_p}{\beta_0}\right)^{2/3} \approx \left(1 + \frac{2}{3}\delta\right)e^{i2m\pi/3},\ m = \{0, 1, 2\}. \tag{A4}$$

Considering the cubic root solution with $m = 0$, the argument in (A3) is simplified to

$$\arg\left(\frac{2V_0\beta_0}{Z_c\beta_p}\left(\left(\frac{\beta_p}{\beta_0}\right)^{2/3}-1\right)^3\right) \approx \pi+3\arg\left(\frac{2}{3}\delta\right) = \pi+3\tan^{-1}\left(\frac{\delta_i}{\delta_r}\right). \quad \text{(A5)}$$

By enforcing angle condition in (A2) to (A5) we obtain

$$\pi+3\tan^{-1}\left(\frac{\delta_i}{\delta_r}\right)=2n\pi,\ \ n=0,\pm1,... \quad \text{(A6)}$$

A relation between δ_r and δ_i is determined by solving (A6) which finally yields three possible solutions

$$\delta_i=\begin{cases}0\\ \sqrt{3}\delta_r\\ -\sqrt{3}\delta_r\end{cases}. \quad \text{(A7)}$$

We neglect the solution $\delta_i = 0$ in (A7) because the regime we are considering has DPE which implies that $\delta_i > 0$. Using the solution $\delta_i = \pm\sqrt{3}\delta_r$ in (A1) will finally find the EPD current to be

$$I_{0e}\approx\frac{2V_0}{Z_{cr}}\left(\frac{2}{3}\left(\delta_r\pm i\sqrt{3}\delta_r\right)\right)^3=\frac{128}{81\sqrt{3}}\frac{V_0\delta_i^3}{(-Z_{cr})} \quad \text{(A8)}$$

Therefore, the EPD condition is met by just tuning the e-beam dc current I_0 to a specific value which we call EPD e-beam current I_{0e}:

$$I_0=I_{0e}\approx\frac{128}{81\sqrt{3}}\frac{V_0}{(-Z_{cr})}\frac{\beta_{pi}^3}{\beta_0^3}\bigg|_{\beta_{pr}=\beta_0}. \quad \text{(A9)}$$

The other two solutions of the cubic root in (A4) with $m = 1$ and $m = 2$ are discarded because they provide solutions for a purely real right hand side of Eq. (A1) for $|\delta_i| > 1$ and $|\delta_r| > 1$, that contradict the initial assumption of $|\delta_r| \ll 1$ and $\delta_i \ll 1$. In summary, the EPD occurs when the e-beam current I_0 takes the value in (A9).

Appendix B: Method used to find the complex-valued wavenumber dispersion of the hybrid hot modes using PIC simulations

We provide the basic steps used to generate dispersion relation of the complex-valued hybrid modes in the hot SWS, and the reader is addressed to [21] for more details. We also provide the details pertaining to the calculations of the equivalent EM voltages and currents in a circular periodic waveguide since this was not discussed in [21].

We define a state vector that describes the EM and space-charge waves at discrete periodic locations $z = z_n = z_{ref} + nd$ as

$$\mathbf{\Psi}_n=[\ V_n,\ \ I_n,\ \ V_{bn},\ \ I_{bn}\ ]^T, \quad \text{(B1)}$$

where $z_{ref} = (d+w)/2$ is located as shown in Fig.10, V_n and I_n are equivalent voltages and currents representing the EM mode in the SWS [22–24], and V_{bn} and I_{bn} are equivalent voltages and currents representing the charge wave modulating the electron beam. We define the voltage and current representing the EM field in the SWS as $V_n = aE_{zn}|_{\rho=0}$ and $I_n = aH_{\phi n}|_{\rho=a}$, respectively, where E_{zn} and $H_{\phi n}$ are field components calculated at discrete periodic locations $z = z_n$, where z_n are z-locations at the beginning of the unit-cells illustrated in Fig. 10. The field in the structure is dominated by theTM_{10} mode which has azimuthal symmetry, i.e., the field component E_{zn} and $H_{\phi n}$are functions of the radial coordinate only, and $a = (R_o + R_i)/2$ is the circular waveguide radius at $z = z_{ref}$. It is important to mention that the locations where the field components are sampled, $z = z_n$, are not located where the ports along the waveguides are, i.e., the waveguide cross-sections at $z = z_n$ are circular, therefore, the field mainly preserves its azimuthal symmetry.

Although a PIC solver calculates the speeds of the discrete large number of charged particles, we represent the longitudinal speed of all electron-beam charges as one dimensional. The beam total equivalent kinetic voltage at the entrance of the n^{th} unit-cell is defined in time domain as $v_{bn}^{tot}(t) = \sqrt{2\eta u_{bn}^{tot}(t)}$, where $u_{bn}^{tot}(t)$ is the average of all the speeds of the charges at each z-cross section (see [5] for more details). The ac modulation is then calculated as $v_{bn}(t) = v_{bn}^{tot}(t) - V_0$, which is then converted to the phasor domain to construct the system's state vector. The term I_{bn} is calculated as the phasor domain transformation of the ac part of the current of the electron beam, at discrete locations $z = z_n = nd$ (see [5] for more details).

In the phasor-domain, we model each unit cell of the interacting SWS as a 4-port network circuit as shown in Fig. 10, and we need to determine its associated transfer matrix. Under the assumption of small signal modulation of the beam's electron velocity and charge density, all the 4-port networks modeling the interaction between the EM and the charge wave in each unit-cell of the hot SWS are assumed identical. Therefore, the single 4×4 transfer matrix $\mathbf{T}_u$ of the interaction unit-cell should satisfy

$$\begin{aligned}\mathbf{\Psi}_2&=\mathbf{T}_u\mathbf{\Psi}_1, && (B2.1)\\ \mathbf{\Psi}_3&=\mathbf{T}_u\mathbf{\Psi}_2, && (B2.2)\\ &\vdots\\ \mathbf{\Psi}_{N+1}&=\mathbf{T}_u\mathbf{\Psi}_N, && (B2.N)\end{aligned} \quad \text{(B2)}$$

where $\mathbf{\Psi}_{n+1}$ and $\mathbf{\Psi}_n$ are the input and output state vectors of the n^{th} unit-cell, respectively, with $n = 1$, 2,.. N. Since the state vectors are calculated using data

from PIC simulations, the relations in (B2) represent $4N$ linear equations in 16 unknowns, which are the unknown elements of the transfer matrix $\mathbf{T}_u$. The system in (B2) is mathematically referred to as overdetermined because the number of linear equations ($4N$ equations) is greater than the number of unknowns (16 unknowns). We rewrite (B2) in matrix form as $[\mathbf{W}_2]_{4\times N} = [\mathbf{T}_u]_{4\times 4}[\mathbf{W}_1]_{4\times N}$. The column of the matrices $\mathbf{W}_1$ and $\mathbf{W}_2$ are the state vectors at input and output, respectively, of each unit-cell and they are written in the form $\mathbf{W}_1 = \left[\ \mathbf{\Psi}_1,\ \mathbf{\Psi}_2,\ \ldots\ \mathbf{\Psi}_N\ \right]$ and $\mathbf{W}_2 = \left[\ \mathbf{\Psi}_2,\ \mathbf{\Psi}_3,\ \ldots\ \mathbf{\Psi}_{N+1}\ \right]$ .. An approximate solution that best satisfies all the given equations in Eq. (B2), i.e., minimizes the sums of the squared residuals, $||\mathbf{W}_2 - \mathbf{T}_u\mathbf{W}_1||^2$ is determined similarly to what was shown in [25–27] and is given by

$$\mathbf{T}_u = \left([\mathbf{W}_2]_{4\times N}[\mathbf{W}_1]^T_{4\times N}\right)\left([\mathbf{W}_1]_{4\times N}[\mathbf{W}_1]^T_{4\times N}\right)^{-1}. \tag{B3}$$

The hybrid eigenmodes are determined by assuming a state vector has the form of $\mathbf{\Psi}_n \propto e^{-jknd}$, where k is the complex-valued Bloch wavenumber that has to be determined and d is the SWS period. Inserting the assumed sate vector z-dependency in (B2), the four Floquet-Bloch modes wavenumbers are determined from the eigenvalue problem

$$e^{-jkd} = \mathrm{eig}(\mathbf{T}_u). \tag{B4}$$

[1] M. V. Berry, Physics of nonhermitian degeneracies, Czechoslovak Journal of Physics **54**, 1039 (2004).

[2] C. M. Bender and S. Boettcher, Real spectra in non-Hermitian Hamiltonians having PT symmetry, Physical Review Letters **80**, 5243 (1998).

[3] S. Klaiman, U. Günther, and N. Moiseyev, Visualization of branch points in p t-symmetric waveguides, Physical Review Letters **101**, 080402 (2008).

[4] M. Liertzer, L. Ge, A. Cerjan, A. Stone, H. E. Türeci, and S. Rotter, Pump-induced exceptional points in lasers, Physical Review Letters **108**, 173901 (2012).

[5] T. Mealy, A. F. Abdelshafy, and F. Capolino, Exceptional point of degeneracy in a backward-wave oscillator with distributed power extraction, Physical Review Applied **14**, 014078 (2020).

[6] T. Mealy, A. F. Abdelshafy, and F. Capolino, Backward-wave oscillator with distributed power extraction based on exceptional point of degeneracy and gain and radiation-loss balance, in *2019 International Vacuum Electronics Conference (IVEC)* (IEEE, 2019) pp. 1–2.

[7] A. Gilmour, *Principles of traveling wave tubes* (Norwood, MA, USA: Artech House, 1994).

[8] B. Levush, T. M. Antonsen, A. Bromborsky, W.-R. Lou, and Y. Carmel, Theory of relativistic backward-wave oscillators with end reflectors, IEEE transactions on plasma science **20**, 263 (1992).

[9] H. R. Johnson, Backward-wave oscillators, Proceedings of the IRE **43**, 684 (1955).

[10] S. Chen, K. Chu, and T. Chang, Saturated behavior of the gyrotron backward-wave oscillator, Physical Review Letters **85**, 2633 (2000).

[11] L. D. Moreland, E. Schamiloglu, W. Lemke, S. Korovin, V. Rostov, A. Roitman, K. J. Hendricks, and T. Spencer, Efficiency enhancement of high power vacuum bwo's using nonuniform slow wave structures, IEEE Transactions on Plasma Science **22**, 554 (1994).

[12] Z.-H. Li, Investigation of an oversized backward wave oscillator as a high power microwave generator, Applied Physics Letters **92**, 054102 (2008).

[13] J. Zhang, H.-H. Zhong, Z. Jin, T. Shu, S. Cao, and S. Zhou, Studies on efficient operation of an x-band oversized slow-wave HPM generator in low magnetic field, IEEE Transactions on Plasma Science **37**, 1552 (2009).

[14] J. Pierce, Waves in electron streams and circuits, Bell System Technical Journal **30**, 626 (1951).

[15] P. A. Sturrock, Kinematics of growing waves, Physical Review **112**, 1488 (1958).

[16] G. W. Hanson, A. B. Yakovlev, M. A. Othman, and F. Capolino, Exceptional points of degeneracy and branch points for coupled transmission lines—Linear-algebra and bifurcation theory perspectives, IEEE Transactions on Antennas and Propagation **67**, 1025 (2019).

[17] A. Welters, On explicit recursive formulas in the spectral perturbation analysis of a jordan block, SIAM Journal on Matrix Analysis and Applications **32**, 1 (2011).

[18] A. Seyranian, O. Kirillov, and A. Mailybaev, Coupling of eigenvalues of complex matrices at diabolic and exceptional points, Journal of Physics A: Mathematical and General **38**, 1723 (2005).

[19] L. Walker, Starting currents in the backward-wave oscillator, Journal of Applied Physics **24**, 854 (1953).

[20] M. A. Othman, V. A. Tamma, and F. Capolino, Theory and new amplification regime in periodic multimodal slow wave structures with degeneracy interacting with an electron beam, IEEE Transactions on Plasma Science **44**, 594 (2016).

[21] T. Mealy and F. Capolino, Traveling wave tube eigenmode solver for interacting hot slow wave structure based on particle-in-cell simulations, arXiv preprint arXiv:2010.07530 (2020).

[22] N. Marcuvitz, *Waveguide handbook* (New York: McGraw-Hill, 1951).

[23] R. E. Collin, *Field theory of guided waves* (John Wiley & Sons, Hoboken, NJ, USA, 1990).

[24] L. B. Felsen and N. Marcuvitz, *Radiation and scattering of waves* (John Wiley & Sons, Hoboken, NJ, USA, 1994).

[25] G. E. Forsythe, Computer methods for mathematical computations., Prentice-Hall series in automatic computation (Englewood Cliffs, NJ, USA, 1977).

[26] G. Williams, Overdetermined systems of linear equations, The American Mathematical Monthly **97**, 511 (1990).

[27] H. Anton and C. Rorres, *Elementary linear algebra: applications version* (John Wiley & Sons, Hoboken, NJ, USA, 2013).